SANDSTONE CONSOLIDATION III
YEAR END REPORT

by
W. R. Kaiser, Kinji Magara
K. L. Milliken and D. R. Richman

Bureau of Economic Geology
The University of Texas at Austin
University Station, Box X
Austin, Texas 78712

Submitted ~~by~~ to

The U.S. Department of Energy
Nevada operations Office
Las Vegas, Nevada

Funded by

DOE Contract No., DE-AC08-79ET27111

January, 1981

SANDSTONE CONSOLIDATION III

YEAR END REPORT

W. R. Kaiser, Kinji Magara, K. L. Milliken, and D. L. Richmann

INTRODUCTION

Two areas of cap rock occurrence have been mapped, one in the upper Texas Coast and the other in South Texas. These may be related to ancient delta systems. Two high resistivity zones have been identified in Brazoria County. The nature of the high resistivity intervals remains enigmatic. Most of the carbonate they contain is microscopically and isotopically skeletal in origin. Few authigenic components have been identified. Isotopic data suggest minimal recycling of pore waters between shale and sandstone.

Hydrolysis reactions and reactions between key pairs of minerals have been written. The goal is to plot formation waters on stability diagrams for these reaction pairs and to correlate log activity ratios with the presence or absence of cap rock and deep secondary porosity. Mineral compositions are based on microprobe data from earlier Sandstone Consolidation projects and new data collected in this project. Methods have been developed to estimate thermodynamic functions for most of these minerals at elevated temperatures. Methods differ depending on the mineral class and availability of published thermodynamic data.

CAP ROCK MAPPING

Cross sections and maps of the shale cap rock (high resistivity zones) have been made from several hundred geophysical logs. Two main areas of cap

rock have been mapped, one in Brazoria-Galveston Counties and the other in Kenedy County. In Brazoria County two high resistivity zones at 7,000 to 8,000 ft and 10,000 to 12,000 ft have been identified. The shallower zone is at the base of the hydropressured interval (0.465 psi/ft) and the deeper one is near the boundary between the soft geopressured and hard geopressured intervals (0.7 psi/ft). The deeper zone is regionally more extensive than the shallower zone.

Geographically, the cap rock appears to coincide with two Frio delta systems, the Houston Delta System on the upper coast and the Norias Delta System in South Texas. It is further suggested that since delta sediments are normally rich in woody and herbaceous organic matter an extraordinary quantity of CO_2 is produced in these areas contributing to cap rock formation. In contrast, interdeltaic areas seem to have no major cap rock development and its absence is believed to be related to a greater abundance of amorphous organic matter.

Data on the percentage of organic carbon have been compiled for the Frio Formation (fig. 1). A histogram shows that most samples range from about 0.1 to 0.4 weight percent with an average of 0.28 percent (fig. 2). The commonly accepted lower limit for significant oil generation in other basins is approximately 0.5 percent.

FLUID FLOW MAPPING

Using digital sonic log data, we plan to map the vertical and horizontal compaction fluid-flow patterns at the present time in Brazoria County. Sonic transit time can be related to porosity or compaction level of shale. Because there is an intimate relationship among the level of shale compaction,

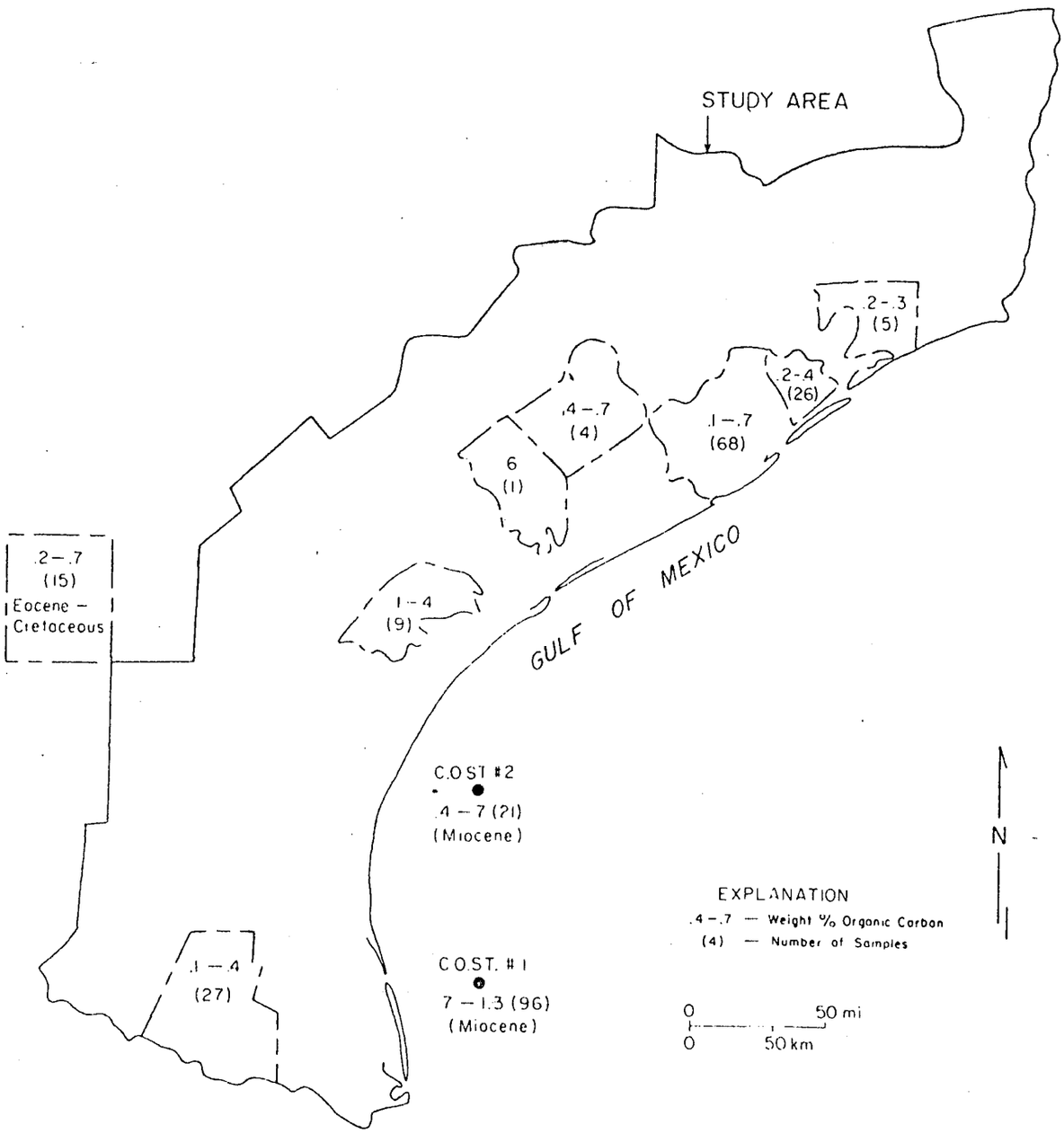

Figure 1. Distribution by county of organic carbon content of shales in the Frio Formation study area and adjacent areas.

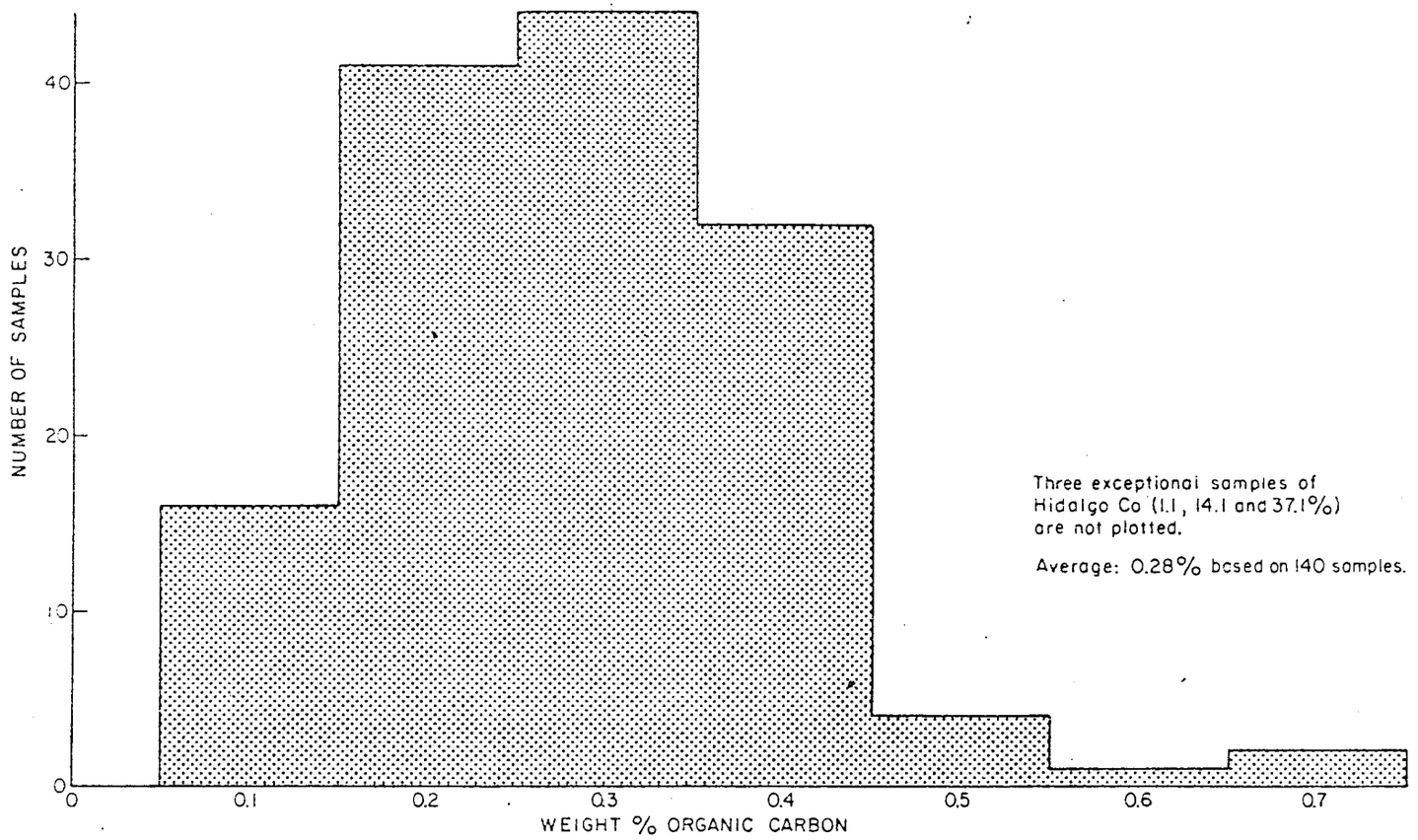

Figure 2. Histogram of organic carbon content in the Frio Formation.

depth of burial, and pore-fluid pressure, it is possible to estimate the pore-fluid pressure at a given depth from the level of shale compaction or shale transit time value (fig. 3). The estimated pore-fluid pressure values in shales may be used to interpret the vertical and horizontal fluid-flow patterns which exist in the subsurface at the present time (fig. 4).

However, fluid-flow patterns in the geologic past are likely to be different from the present patterns. This is because the paleo fluid-flow is controlled mainly by the loading patterns and the fluid-expulsion efficiency of the sedimentary sequences. Whether or not a given sedimentary sequence retained relatively high efficiency for fluid expulsion in the geological past can be evaluated by the comparison of the sediment's total loading pressure and of the remaining pore-fluid pressure. If most of the loading pressure has been relieved due to effective fluid expulsion, it would now have relatively low pressure. Such a sedimentary unit would indicate very little movement of fluids at present, but must have experienced significant fluid expulsion and movement in the geologic past. The objective of the paleo and present fluid-flow analyses is to indicate the direction of movement of fluids containing mineral solutes and to infer the likely places for precipitation of minerals.

In summary, the paleo and the present fluid-flow patterns must be analyzed separately. For the paleo fluid-flow study, a loading map (map showing the total weight of sedimentary column) can be constructed and used. For the present fluid-flow study, the pressure values derived from the analysis of sonic transit time can be used.

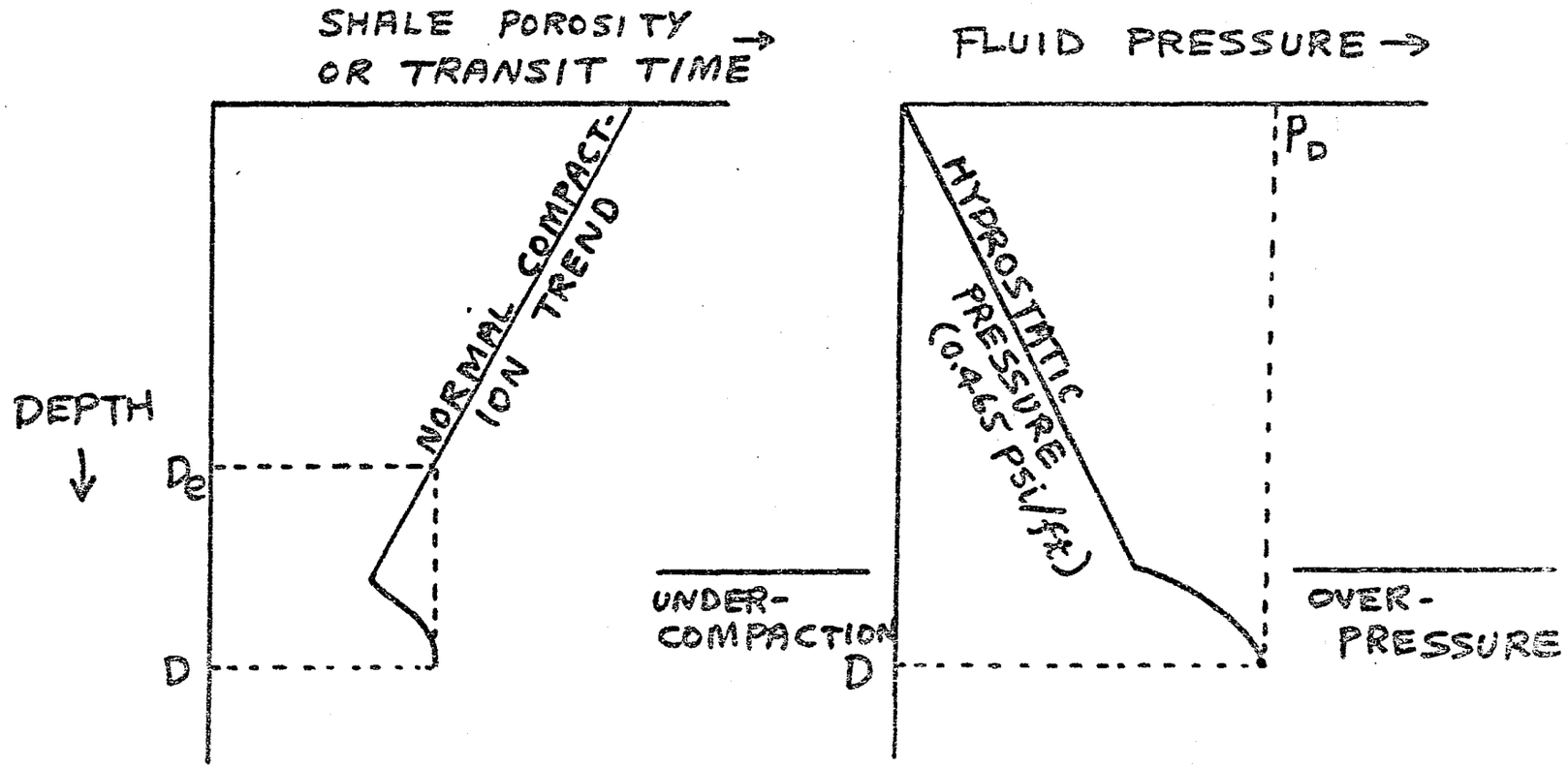

$$P_D\,(psi) = 0.465 \times D_e + 1 \times (D - D_e)$$

[D AND De IN FEET]

Figure 3. Schematic diagrams showing shale porosity or transit time versus depth and fluid pressure versus depth relationships. Equation is for calculating fluid pressure at depth D in an undercompacted interval.

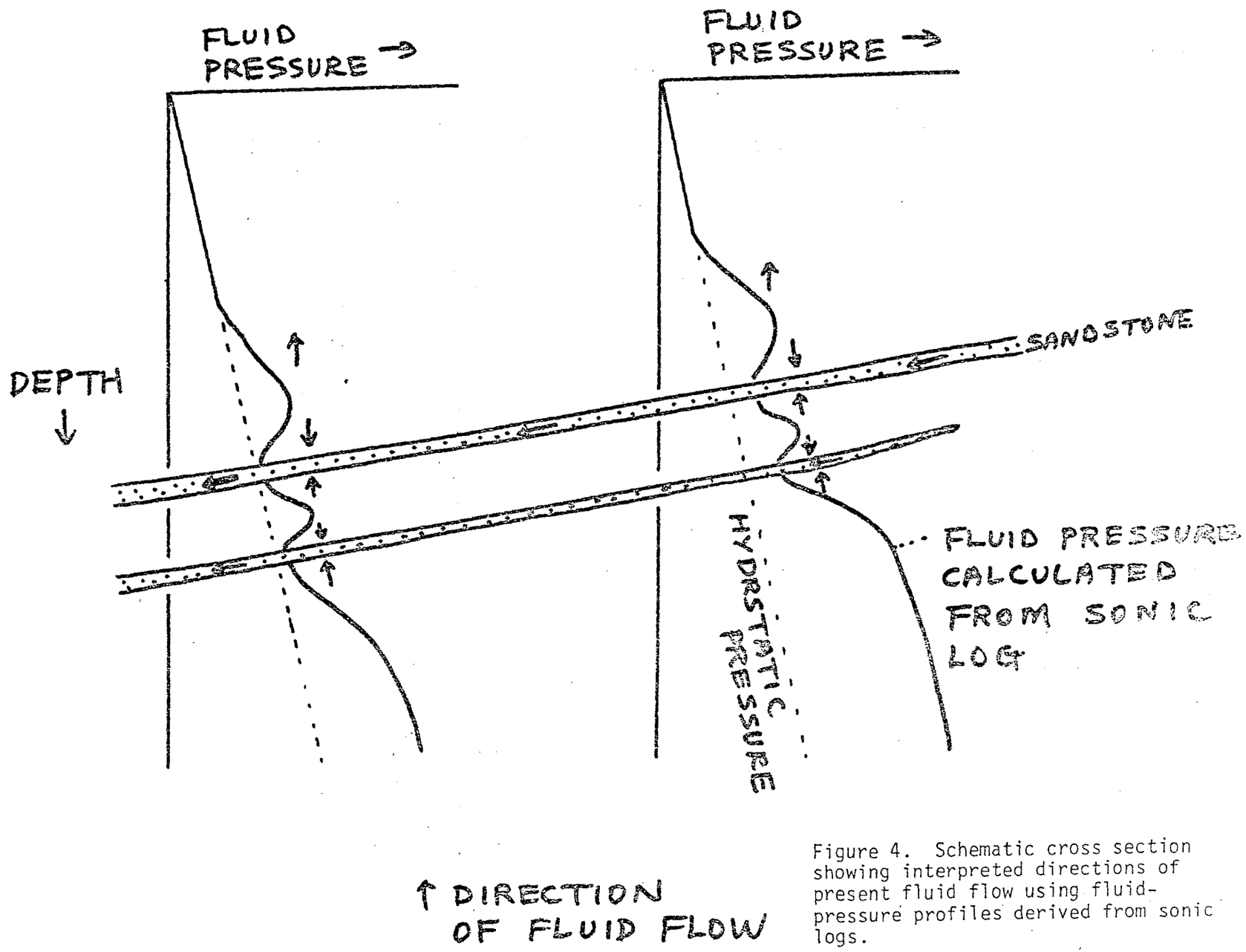

Figure 4. Schematic cross section showing interpreted directions of present fluid flow using fluid-pressure profiles derived from sonic logs.

CAP ROCK PETROLOGY

Background

Heretofore, no one has conducted detailed petrographic analyses of cap rock in order to explain its response on geophysical logs; i.e., why do resistivities within cap rock zones increase so abruptly? Is this effect related to shale mineralogy, pore fluids, or some other feature of the cap rock?

It is known that cap rock consists of calcareous shale, but the nature of the carbonate material contained within the shale has never been documented. One of the major objectives of this study is to determine the genetic association of these carbonates. If they prove to be authigenic and if it can be shown that cap rock resistivity is related to their presence, then the distribution of cap rock, cemented with material possibly leached from the underlying strata, could bear some relationship to deep secondary reservoirs. On the other hand, if resistivity cannot be related to the presence of authigenic carbonate (or other authigenic minerals) some other physical or chemical parameter must control it.

Sampling and Analytical Techniques

On the basis of shale resistivity and interval transit time plots, cap rock intervals were identified in three wells from Brazoria County; GCO/DOE No. 2 Pleasant Bayou, Humble No. 1 J. M. Skrabanek, and Humble No. 1 R. W. Vieman. In all three wells, a shallow and a deeper high-resistivity cap rock zone was identified. Whole-core samples from the intervals of interest were not available; however, we obtained washed cuttings from these wells over portions of each cap rock interval and from the section above and below these intervals.

from the washed cuttings a pure shale sample of about 5 grams was hand picked under the binocular microscope. These shale cuttings were examined on the scanning electron microscope (SEM) as whole rock fragments and in ultrasonically disaggregated size fractions. In addition, disaggregated samples in liquid mounts were examined with a standard polarizing microscope.

The sole petrographic criterion we used to identify authigenic minerals was crystal morphology. By analogy to coarser-grained sediments, authigenic phases typically develop euhedral crystal faces where they grow into pore space. Thus, we would expect that authigenic carbonates present in the shales might occur as recognizable rhombs.

Preliminary Results

Identification of individual constituents of the cap rock is best accomplished using disaggregated samples. In the whole cuttings, many of the constituents were impossible to identify without the energy dispersive analyzer (EDA) because of dense coatings of detrital clay that obscured their morphology. This problem was largely alleviated by using the disaggregated samples.

Disaggregated samples were examined in the following size fractions: <2μm; 2 to 20 μm; >20μm; and whole sample. Most of our data were obtained from observations of the >20μm and 2 to 20 μm size fractions. In these splits, we found that skeletal carbonate, consisting of coccolith and foraminifer fragments, comprises a significant portion of the sample (figs. 5 and 6). In fact, in the shallow cap rock zones of all three wells, it is the only form of carbonate that could be positively identified by SEM. The detailed structures of the foraminifers and coccoliths are remarkably well preserved. High magnification views of these features (figs. 7 and 8) fail to reveal any evidence of diagenetic modification.

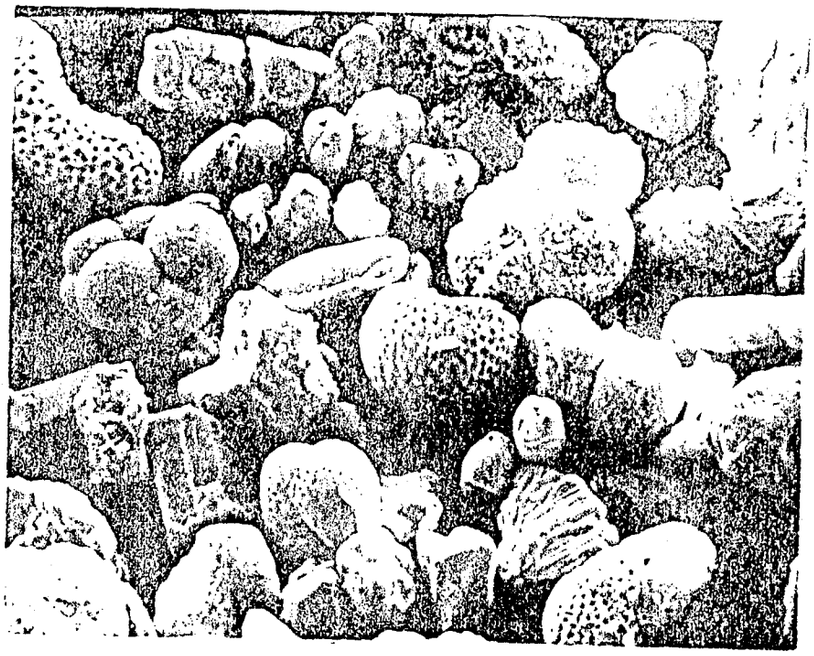

Figure 5. Foraminifers. Foraminifera tests comprise a significant portion of the >20 μm fraction; 9260 - 9290 ft, GCO/DOE #2 Pleasant Bayou.

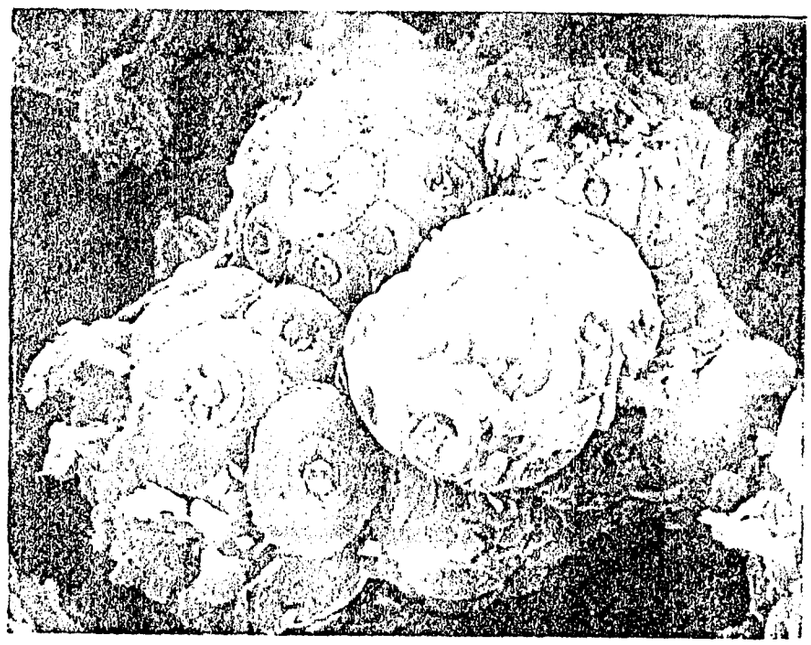

Figure 6. Coccolithophores. Coccoliths, often in the form of entire coccospheres, are abundant in the 2-20 μm fraction; 9716 ft; Humble #1 Vieman. 3700x

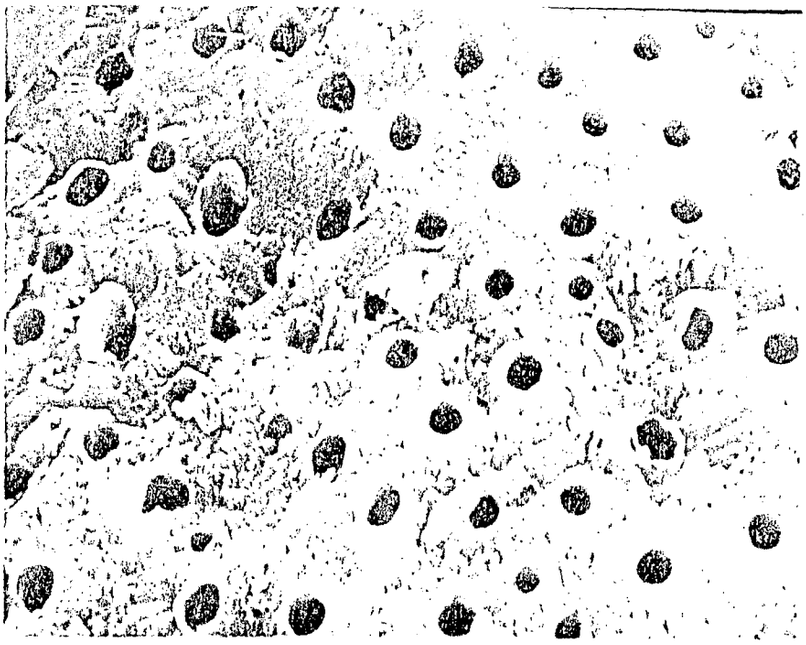

Figure 7. Detailed views of forams reveal no evidence of dissolution or precipitation of authigenic minerals in pores; 6937 ft; Humble #1 Skrabanek. 5100x

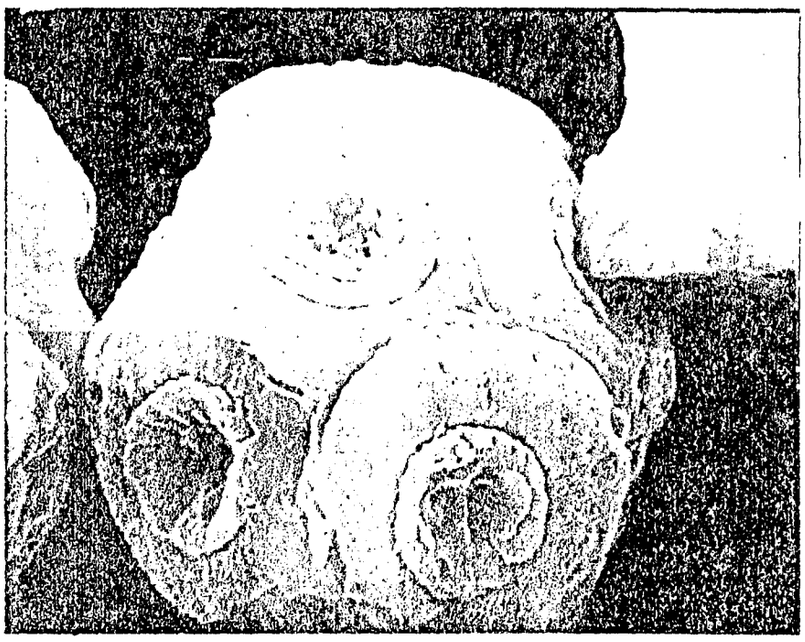

Figure 8. Close examination of coccoliths also reveals little evidence of textural modification from diagenesis; 10,010 ft; GCO/DOE #2 Pleasant Bayou; 4900x

Under the petrographic microscope, some micritic fragments were also observed; these may represent the lithified product of carbonate mud present in the depositional environment. However, these fragments are volumetrically less abundant than fossils.

In some samples from the deeper cap rock zones in each of the three wells, minor quantities of a rhombic mineral were observed (figs. 9a and 9b). These rhombs are iron-bearing carbonate. In all instances where the rhombic carbonates were observed, they occur in extremely minor quantities and are far less abundunt than the skeletal carbonate. Also, there are some problems in interpreting the genesis of these carbonates based only on their form. First, they are too large to have formed as a pore-filling cement. Most are tens of microns across and are thus unlikely to have formed in micropores (on the order of 0.1μm) between the clay flakes of a compacted shale. This does not, however, exclude the possibility that they may have formed authigenically within fractures, as an alteration of detrital material, or within foraminifer chambers. The only clearly authigenic mineral that we have found to occur abundantly in the coarse fractions of the shales is pyrite occurring as framboids.

It is interesting that the consolidation state of the shale does not appear to differ between cap rock and non-cap rock intervals. All samples shallower than 13,000 ft are virtually unlithified and disaggregate spontaneously on contact with water. Below this depth lithification proceeds rapidly with increasing depth to form very hard, splintery, slate-like shales. The transition to lithified shale roughly corresponds to the total loss of carbonate with depth (fig. 10) and stabilization of mixed layer illite/smectite at approximately 80 percent illite layers (Freed, 1980). Intergrowth of clay flakes may be responsible for the increasing lithification.

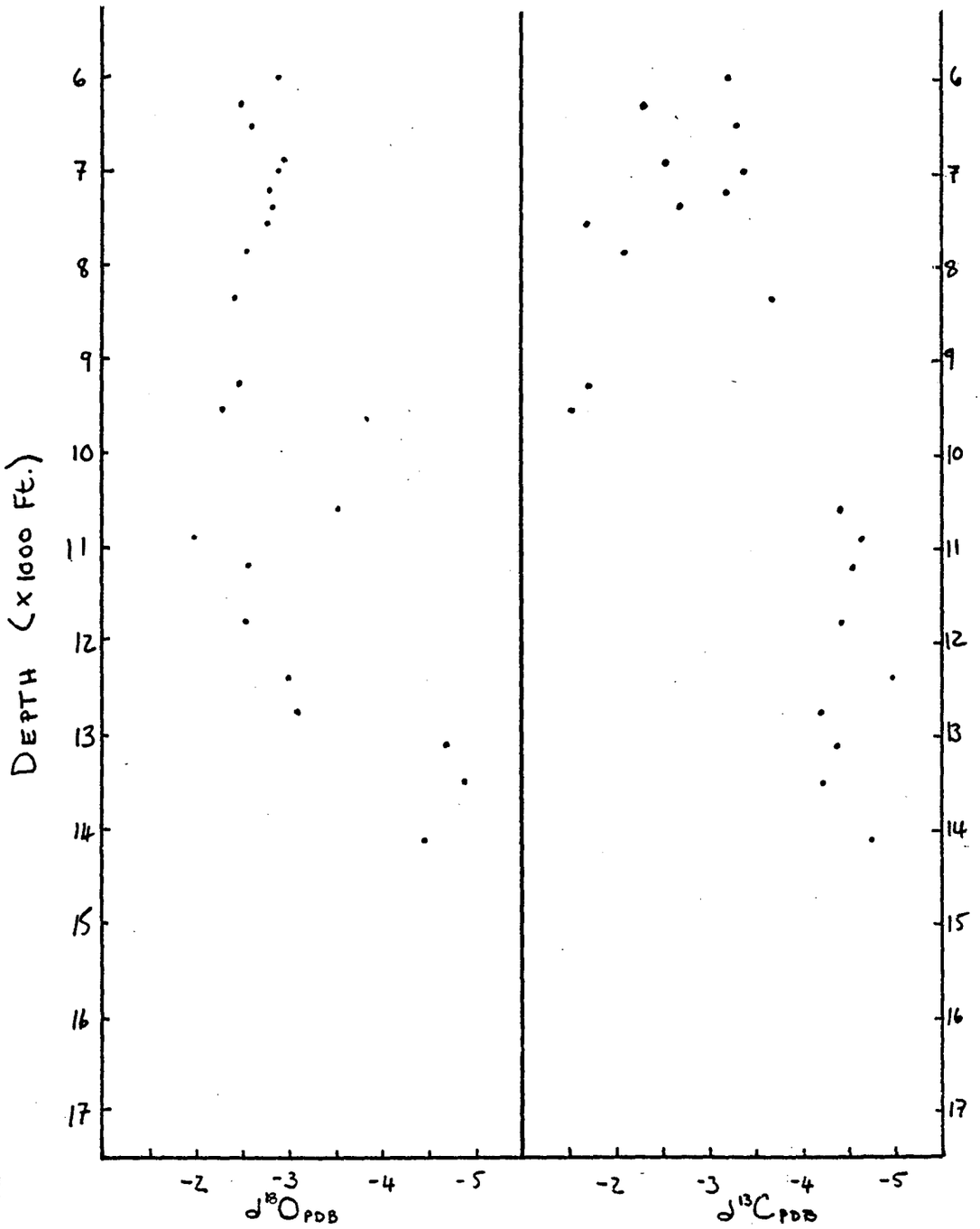

Figure 11. Bulk carbonate oxygen and carbon isotopic data versus depth, Brazoria County shales. No carbonate below 14,000 ft.

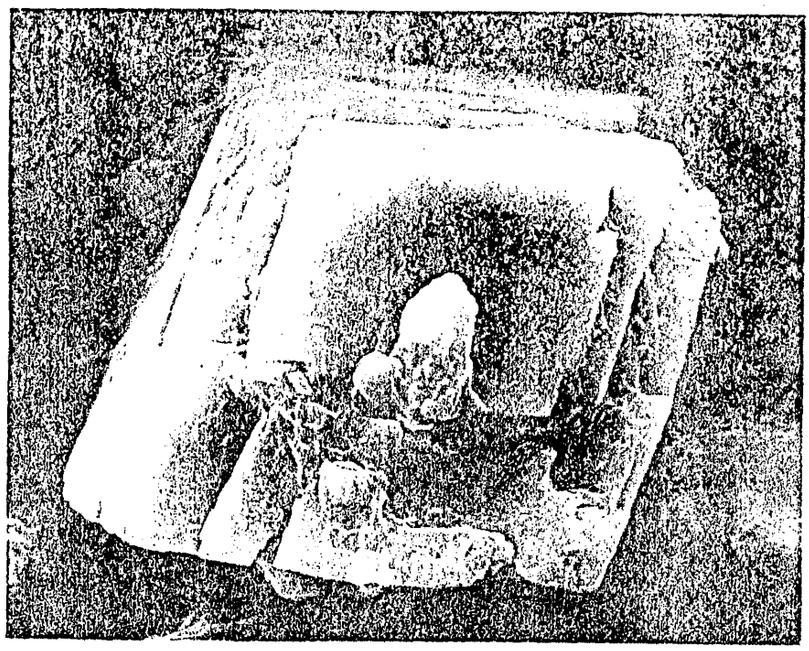

Figure 9a. Single rhomb (Fe-bearing carbonate); 10,010 ft; GCO/DOE #2 Pleasant Bayou; 3200x.

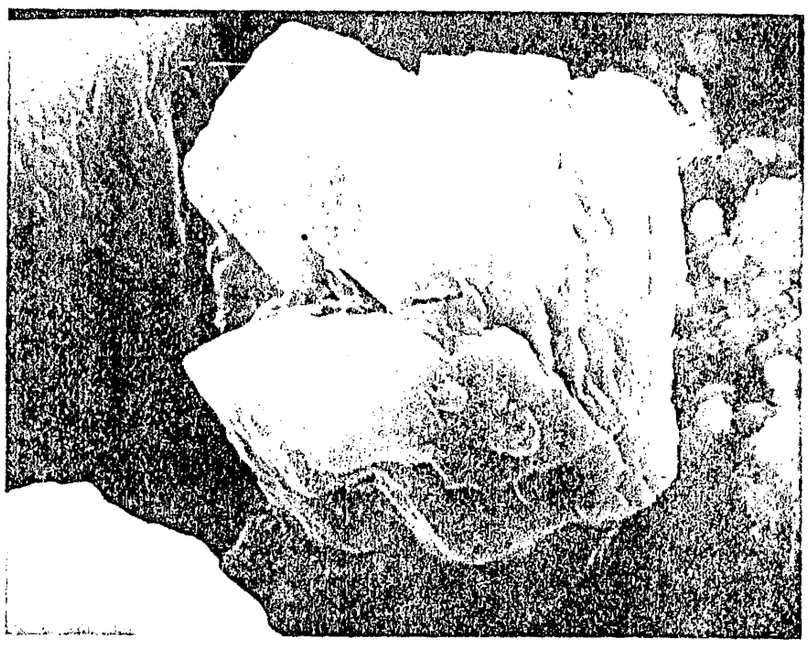

Figure 9b. Cluster of rhombs; 10,010 ft, GCO/DOE #2 Pleasant Bayou; 5200 x.

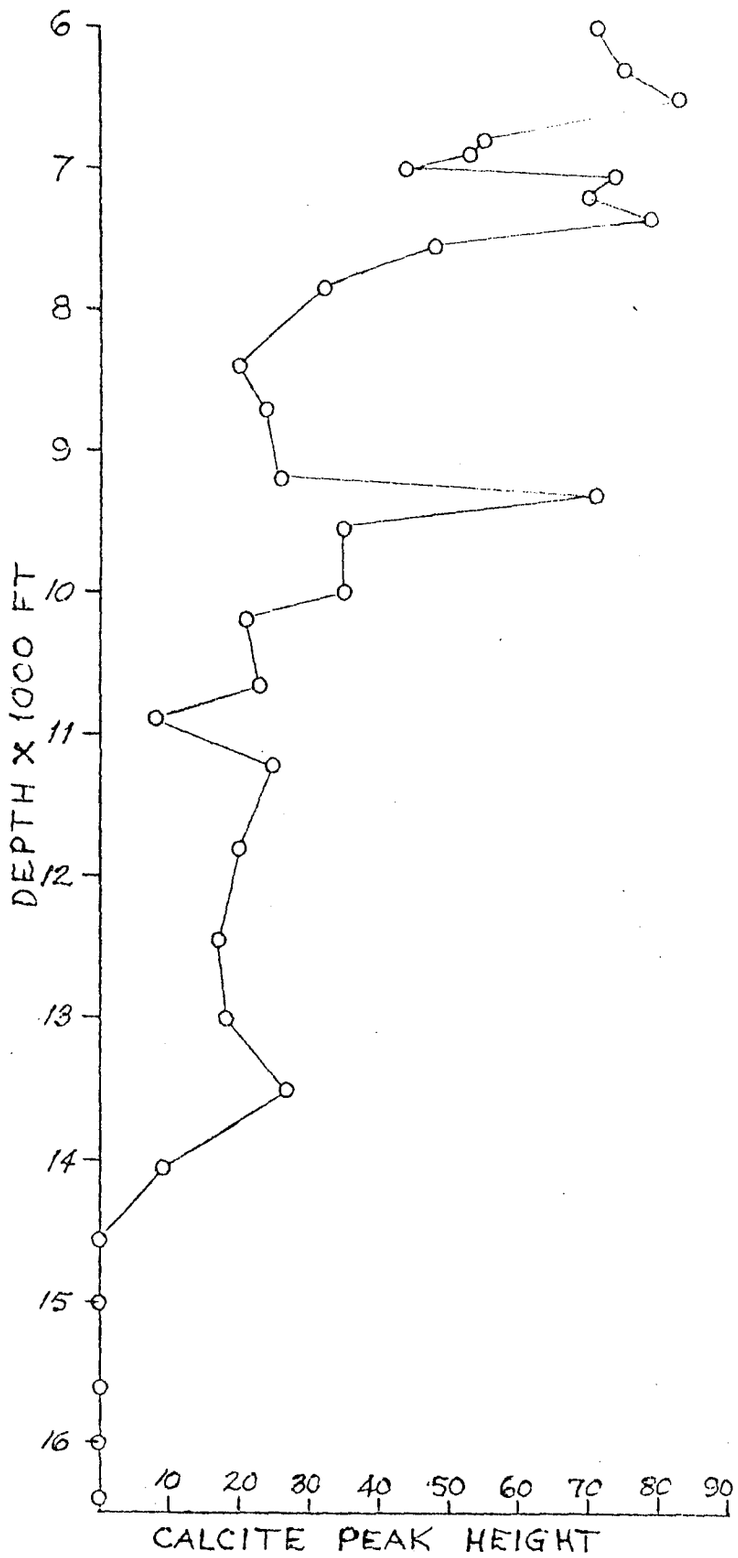

Figure 10. Calcite peak height from X-ray diffractometer traces versus depth, Brazoria County shales. Hard, splintery shale occurs below 14,000 ft.

ISOTOPE GEOCHEMISTRY

Twenty-two shale samples from the same three wells in the Chocolate Bayou Field have been analyzed for oxygen and carbon isotopes. To obtain CO_2 gas for isotopic analysis, carbonate in the bulk shale sample is reacted under vacuum with 100 percent anhydrous phosphoric acid. Gases have been extracted from other samples and these will be analyzed. Shale samples for isotopic analysis are selectively removed from cuttings by hand picking, ground in a ceramic mortar and X-rayed to determine the number of carbonate phases present and their relative abundance. All Brazoria County samples examined so far are calcite.

Isotopic data obtained so far are consistent with a carbonate fraction consisting primarily of skeletal debris (fig. 11; table 1). At all depths examined $\delta^{18}O$ values for carbonates in shales are significantly heavier than the $\delta^{18}O$ values for carbonates in associated sandstones (Loucks, Richmann, Milliken, 1980) and is consistent with minimal recycling of pore waters between shale and sandstone. In other words, waters were squeezed out of the shales into the sandstones and underwent minor recontact with the shales. Both sandstones and shales have a shift toward lighter $\delta^{13}C$ values at approximately 10,000 ft. The shift in the sandstones, however, is to values of approximately -10 per mil whereas values in shales below 10,000 ft were approximately -5 per mil. Below approximately 12,500 ft $\delta^{13}C$ values in sandstones become heavier whereas $\delta^{13}C$ values in shales do not show a trend toward heavier values (fig. 11).

Above approximately 10,000 ft $\delta^{18}O$ and $\delta^{13}C$ values of shale carbonates are consistent with essentially unmodified skeletal debris. Below this depth isotopic values are still within the range of values possible for skeletal

Table 1. Brazoria County Isotope Data

Well Name	Sample No.	Depth (ft)	$\delta^{18}O$	$\delta^{13}C$
GCO/DOE #2 Pleasant Bayou	BrS-1	9260 - 9290	-2.44	-1.73
" " " "	BrS-2	9520 - 9580	-2.30	-1.59
" " " "	BrS-3	10,010 - 10,040		
" " " "	BrS-4	10,650 - 10,680	-3.54	-4.41
" " " "	BrS-5	11,220 - 11,250	-2.58	-4.54
" " " "	BrS-6	11,800 - 11,840	-2.53	-4.41
" " " "	BrS-7	12,410 - 12,440	-3.02	-4.98
" " " "	BrS-8	13,050 - 13,090	-4.67	-4.38
" " " "	BrS-9	13,510 - 13,540	-4.84	-4.22
" " " "	BrS-10	14,110 - 14,140	-4.46	-4.75
Humble #1 Skrabanek	BrS-16	6874 - 6906	-2.95	-2.54
" " "	BrS-17	6998 - 7030	-2.89	-3.38
" " "	BrS-18	7184 - 7215	-2.54	-3.18
" " "	BrS-19	7336 - 7367	-2.82	-2.70
" " "	BrS-20	7547 - 7576	-2.77	-1.70
" " "	BrS-21	7834 - 7865	-2.61	-2.11
" " "	BrS-22	8361 - 8393	-2.43	-3.67
" " "	BrS-23	9212 - 9242		
Humble #1 Vieman	BrS-24	6000 - 6028	-2.905	-3.275
" " "	BrS-24a	6000 - 6028		
" " "	BrS-25	6278 - 6308	-2.49	-2.28
" " "	BrS-26	6522 - 6553	-2.60	-3.28
" " "	BrS-26a	6522 - 6554		
" " "	BrS-27	6740 - 6987		
" " "	BrS-28	6987 - 7019		
GCO/DOE #1 Pleasant Bayou	BrS-29	10,240 - 10,260		
" " " "	BrS-30	10,900 - 10,930	-1.99	-4.685
" " " "	BrS-31	12,740 - 12,770	-3.11	-4.20
Humble #1 Skrabanek	BrS-32	8716 - 8745		

debris but show a trend toward somewhat lighter values with depth. Below approximately 14,000 ft the shales are devoid of carbonate. The shift toward lighter isotopic values below 10,000 ft probably reflects increased amounts of exchange between carbonate particles and shale pore fluids at higher temperature.

DETRITAL FELDSPAR COMPOSITION

Background

The Sandstone Consolidation III project includes microprobe analysis of: (1) detrital feldspars - to assess the potential consequences of albitization on sandstone diagenesis, and (2) authigenic carbonates - to determine whether any systematic or sequential variations in carbonate chemistry can be documented, and if so, what the implications of such variations are. Because of unforeseen operational problems with, and only limited access to the University of Texas Geology Department's microprobe, this part of the project has only recently been initiated and resulting data are very preliminary.

We have not yet begun analysis of carbonates, but are currently analyzing detrital feldspars from Miocene, and Oligocene Frio sandstones from Brazoria County, Texas. On completion of this part of the task, we will conduct similar analyses of feldspars in Vicksburg sandstones from Hidalgo County, Texas and compare the two data sets. This comparison may tell us if the albitization reaction is dominantly temperature-dependent (since Upper and Lower Texas Gulf Coast regions are characterized by differing geothermal gradients) or if other factors are significant controls (e.g., whether a "threshold" anorthite content of detrital plagioclase is requisite to albitization; the potential effect of depositional matrix on the reaction; and in light of concurrent

research on brine chemistry, what the influence of variable pore fluid compositions might be).

Sampling and Analytical Techniques

Probe sections were made from whole-core, and from hand-picked sandstone cuttings over depth intervals where core was unavailable. This was done to obtain the most continuous depth distribution of samples possible. Samples were ideally taken every 50 to 100 feet; however, natural sampling gaps exist due to the distribtuion of sand bodies within the sedimentary sequence.

Fifty-three polished probe sections were made from Brazoria County samples. Sample depths range from 4,345 ft to 17,783 ft. Acquisition of samples from the Lower Texas Coast is not yet complete. At present, we have 28 polished sections of Vicksburg sandstones from Hidalgo County.

Microprobe analyses are conducted on an Applied Research Laboratories instrument utilizing an energy dispersive spectrometer. Each section is examined in reflected light and 20 randomly selected detrital feldspar grains are analyzed for Na_2O, Al_2O_3, SiO_2, K_2O, CaO, and FeO. Resulting data are printed out as weight percent, and values of the three feldspar end members, An ($CaAl_2Si_2O_8$), Ab ($NaAlSi_3O_8$), and Or ($KAlSi_3O_8$) are normalized to 100 percent by the EDS ULTIMATE program. These end member compositions are then plotted on triangular graphs from which potential compositional trends can be readily distinguished.

Preliminary Results

Thus far, only 2 Miocene samples and 2 Frio samples from the 10,000 ft interval have been analyzed. Preliminary data suggest that the Miocene sandstones and Frio sandstones may have been derived, at least in part, from

different sources. On An-Ab-Or plots overprinted with the fields of plutonic/metamorphic and volcanic feldspar compositions (from Trevena and Nash, unpublished manuscript), detrital feldspar compositions from the Miocene samples are all consistent with a plutonic/metamorphic source (fig. 12). In contrast, a number of feldspars from the Frio samples can only be accounted for by a volcanic source (fig. 13). While, admittedly, these differences could be attributed to the overlap in the feldspar fields, this seems unlikely. The difference in compositional distributions could be attributed to the overlap of the two genetic fields. There is sufficient overlap to interpret a volcanic as well as a plutonic/metamorphic source for the Miocene samples. However, this seems unlikely; one would expect to find some distinctively volcanic feldspar compositions if a volcanic source was contributing significant sediment during the Miocene.

We had originally proposed to use the feldspar mix of the shallow Miocene samples to establish an initial calcium content in order to test subsequent changes in feldspar chemistry resulting from progressive burial and albitization. Since we now believe different sediment sources were involved during deposition of the Miocene and Oligocene Frio sediments, we instead plan to use shallow, poikilotopically cemented Frio sandstones. Our preliminary data suggest that the early poikilotopic calcite cements are impermeable to the albitizing fluids. Consequently, in samples where these cements were not leached prior to burial to depths where albitization occurs, they preserved the original feldspar compositions.

In the Frio samples from the 10,000-ft interval, detrital plagioclase compositions vary from An_1 to An_{63} (fig. 13). This range is considerably greater than expected and could complicate determination of a meaningful average initial calcium content if the feldspar compositions have a large standard deviation.

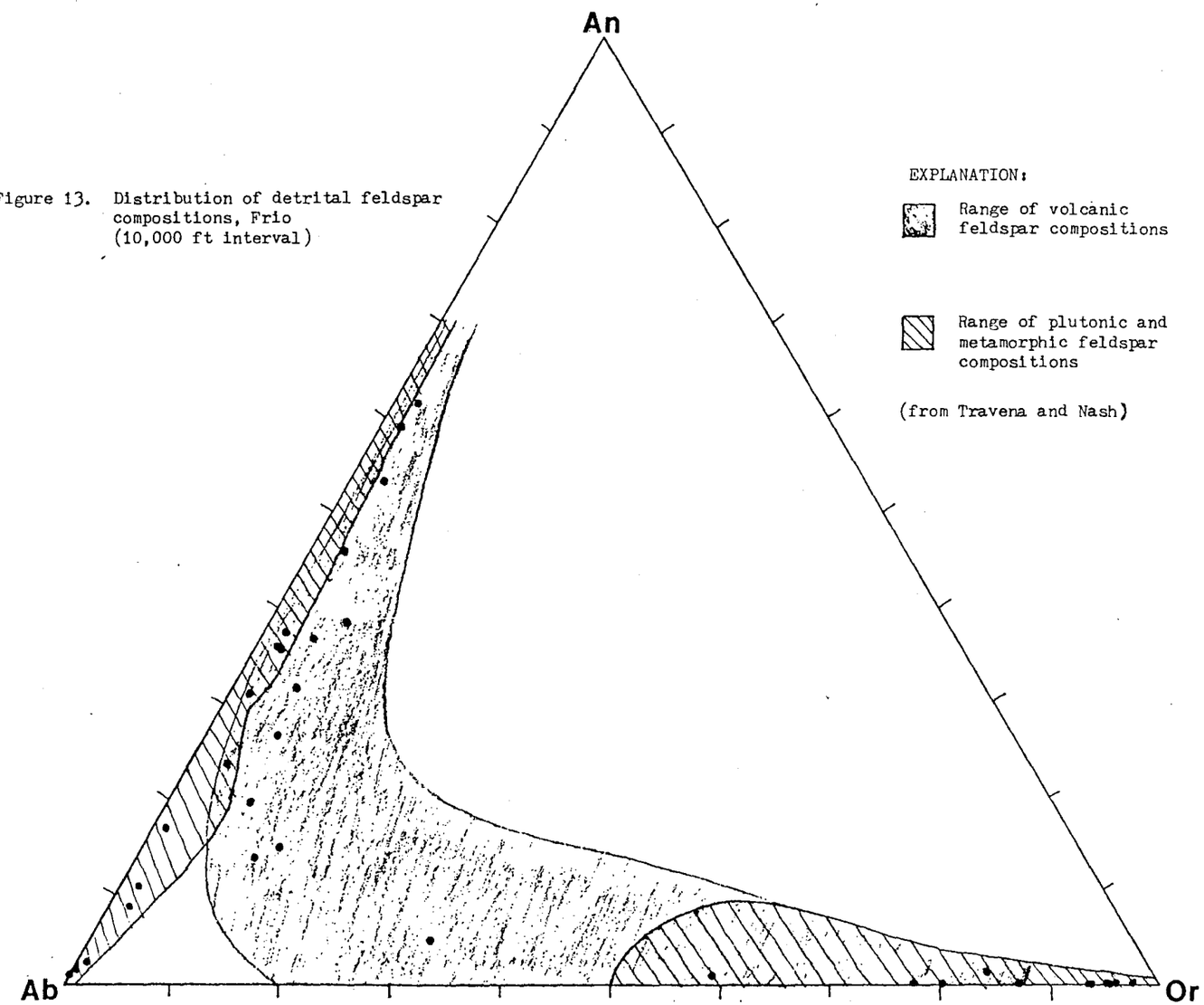

Figure 13. Distribution of detrital feldspar compositions, Frio (10,000 ft interval)

Figure 12. Distribution of detrital feldspar compositions, Miocene

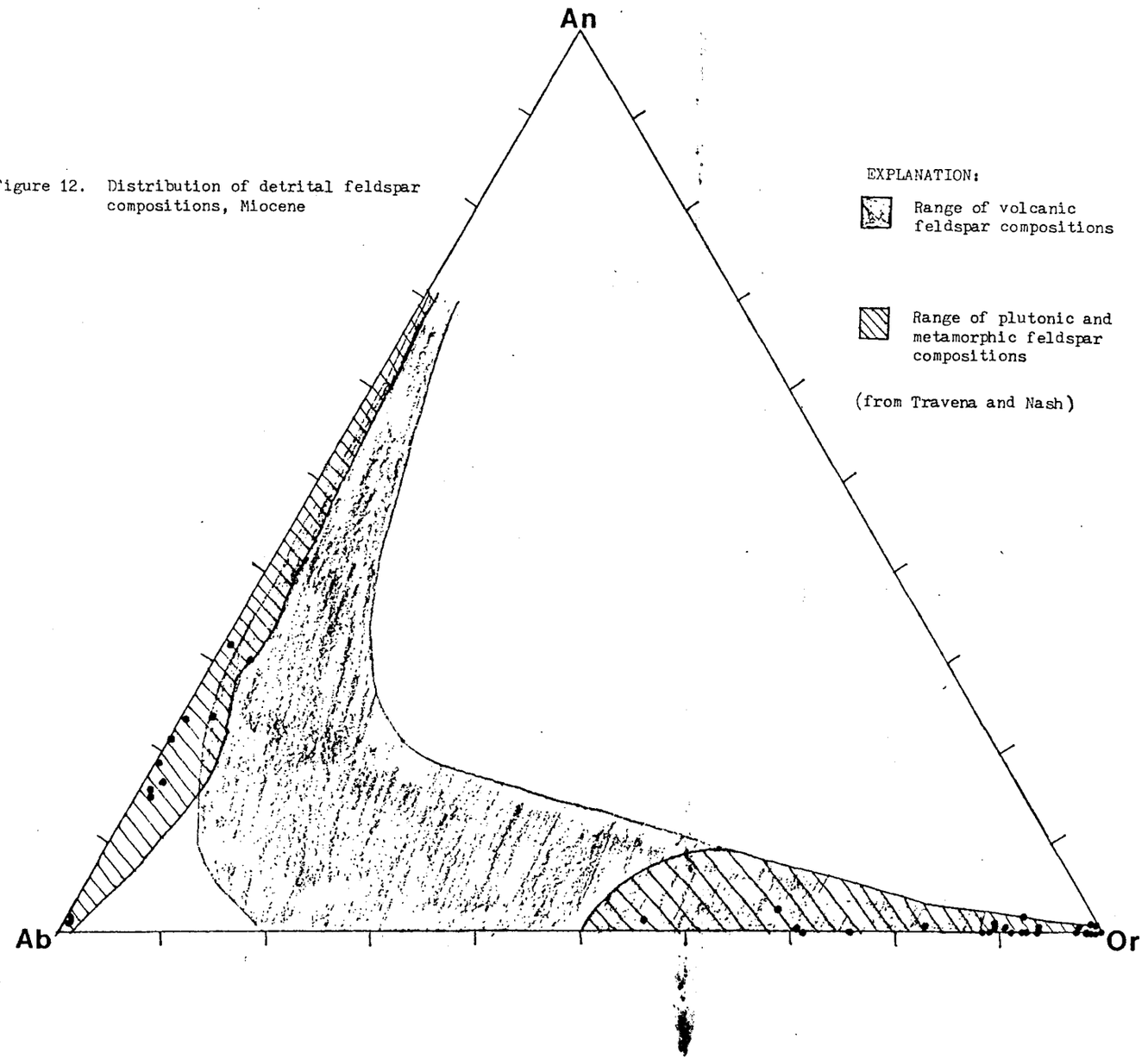

ESTIMATING THERMODYNAMIC FUNCTIONS

Thermodynamic data are directly available for construction of many stability diagrams of fair to excellent validity at 25°C (298.15°K). To calculate stability relations among minerals at higher temperatures, between 25 and 200°C, requires data at the temperature of interest. Ideally, tables of the change in standard free energies of formation ($\Delta G°_f$) would be available at higher temperatures in intervals convenient for interpolation. Because of the fragmentary nature and lack of availability of thermodynamic data no comprehensive compilation has been made, especially for the phyllosilicates or layer silicates. However, enough data has been published to allow estimation of $\Delta G°_f$ for key minerals (table 2) and reactions in tables 3 and 4. The approach is eclectic and is illustrated by calculation of the change in free energies of formation for Ca-montmorillonite and ferroan calcite (table 2).

Ca-Montmorillonite

A method suggested by Helgeson (per. comm., 1971) is used here because it enables estimation of thermodynamic functions at temperatures greater than 25°C. The standard change in enthalpy of formation ($\Delta H°_f$) for Ca-montmorillonite is estimated graphically from a curve derived from phyllosilicates in general (fig. 14). For the ordinate, the change in enthalpy of formation of a particular phyllosilicate is divided by the total number of tetrahedrally coordinated Si and Al atoms ($Si_{Tet}+Al_{Tet}$). The values along the abscissae are obtained by considering octahedral and exchangeable ionic constituents and hydroxyl ions. The enthalpies of formation of these species in aqueous solution, multiplied by their respective stoichiometric coefficients are summed

Table 2. Compositions of key minerals

1. Quartz SiO_2
2. Calcite $CaCO_3$
3. Ferroan calcite $Ca_{.95}Fe_{.05}CO_3$
4. Albite $NaAlSi_3O_8$
5. K-feldspar $KAlSi_3O_8$
6. Intermediate plagioclase $Na_{.7}Ca_{.3}Al_{1.3}Si_{2.7}O_8$
7. Kaolinite $Al_2Si_2O_5(OH)_4$
8. Chlorite $Mg_{2.3}Fe_{2.3}Al_{2.8}Si_{2.6}O_{10}(OH)_8$
9. Ca-montmorillonite $Ca_{.16}(Al_{1.56}Mg_{.25}Fe_{.25})Si_4O_{10}(OH)_2$
10. Na-montmorillonite $Na_{.33}(Al_{1.56}Mg_{.25}Fe_{.25})Si_4O_{10}(OH)_2$
11. Illite $K_{.6}Mg_{.25}Al_{2.3}Si_{3.5}O_{10}(OH)_2$
12. Laumontite $CaAl_2Si_4O_{12} \cdot 4H_2O$
13. Clinoptilolite $NaAlSi_5O_{12} \cdot 4H_2O$
14. Sphene $Ca(Ti_{.7}Al_{.4})SiO_5$

Table 3. Hydrolysis reactions

1. $SiO_2 + 2\ H_2O = H_4SiO_4^\circ$
2. $CaCO_3 = Ca^{2+} + CO_3^{2-}$
3. $Ca_{.95}Fe_{.05}CO_3 = 0.95\ Ca^{2+} + 0.05\ Fe^{2+} + CO_3^{2-}$
4. $NaAlSi_3O_8 + 8\ H_2O = Na^+ + Al(OH)_4^- + 3\ H_4SiO_4^\circ$
5. $KAlSi_3O_8 + 8\ H_2O = K^+ + Al(OH)_4^- + 3\ H_4SiO_4^\circ$
6. $Na_{.7}Ca_{.3}Al_{1.3}Si_{2.7}O_8 + 8\ H_2O = 0.7\ Na^+ + 0.3\ Ca^{2+} + 1.3\ Al(OH)_4^- + 2.7\ H_4SiO_4^\circ$
7. $Al_2Si_2O_5(OH)_4 + 7\ H_2O = 2\ Al(OH)_4^- + 2\ H_4SiO_4^\circ + 2\ H^+$
8. $Mg_{2.3}Fe_{2.3}Al_{2.8}Si_{2.6}O_{10}(OH)_8 + 3.6\ H_2O + 6.4\ H^+ = 2.3\ Mg^{2+} + 2.3\ Fe^{2+} + 2.8\ Al(OH)_4^- + 2.6\ H_4SiO_4^\circ$
9. $Ca_{.16}(Al_{1.56}Mg_{.25}Fe_{.25})Si_4O_{10}(OH)_2 + 10.24\ H_2O = 0.16\ Ca^{2+} + 1.56\ Al(OH)_4^- + 0.25\ Fe^{2+} + 0.25\ Mg^{2+} + 4\ H_4SiO_4^\circ + 0.24\ H^+$
10. $Na_{.33}(Al_{1.56}Mg_{.25}Fe_{.25})Si_4O_{10}(OH)_2 + 10.24\ H_2O = 0.33\ Na^+ + 1.56\ Al(OH)_4^- + 0.25\ Mg^{2+} + 0.25\ Fe^{2+} + 4\ H_4SiO_4^\circ + 0.24\ H^+$
11. $K_{.6}Mg_{.25}Al_{2.3}Si_{3.5}O_{10}(OH)_2 + 11.2\ H_2O = 0.6\ K^+ + 2.3\ Al(OH)_4^- + 3.5\ H_4SiO_4^\circ + 0.25\ Mg^{2+} + 1.2\ H^+$
12. $CaAl_2Si_4O_{12} \cdot 4\ H_2O + 8\ H_2O = Ca^{2+} + 2\ Al(OH)_4^- + 4\ H_4SiO_4^\circ$
13. $NaAlSi_5O_{12} \cdot 4\ H_2O + 8\ H_2O = Na^+ + Al(OH)_4^- + 5\ H_4SiO_4^\circ$
14. $Ca(Ti_{.7}Al_{.4})SiO_5 + 2\ H_2O + 2.3\ H^+ = Ca^{2+} + 0.7\ TiOOH^+ + 0.4\ Al(OH)_4^- + H_4SiO_4^\circ$

Table 4. Reaction pairs

1. $CaCO_3 + 0.05\ Fe^{2+} = Ca_{.95}Fe_{.05}CO_3 + 0.05\ Ca^{2+}$

2. $2\ KAlSi_3O_8 + 2\ H^+ + 9\ H_2O = Al_2Si_2O_5(OH)_4 + 2\ K^+ + 4\ H_4SiO_4^\circ$

3. $KAlSi_3O_8 + Na^+ = NaAlSi_3O_8 + K^+$

4. $Na_{.7}Ca_{.3}Al_{1.3}Si_{2.7}O_8 + 0.6\ Na^+ + 1.2\ H_4SiO_4^\circ = 1.3\ NaAlSi_3O_8 + 0.3\ Ca^{2+} + 2.4\ H_2O$

5. $Na_{.7}Ca_{.3}Al_{1.3}Si_{2.7}O_8 + 1.3\ H^+ + 3.45\ H_2O = 0.65\ Al_2Si_2O_5(OH)_4 + 0.3\ Ca^{2+} + 0.7\ Na^+ + 1.4\ H_4SiO_4^\circ$

6. $1.4\ Al_2Si_2O_5(OH)_4 + 2.3\ Mg^{2+} + 2.3\ Fe^{2+} + 6.2\ H_2O = Mg_{2.3}Fe_{2.3}Al_{2.8}Si_{2.6}O_{10}(OH)_8 + 0.2\ H_4SiO_4^\circ + 9.2\ H^+$

7. $Ca_{.16}(Al_{1.56}Mg_{.25}Fe_{.25})Si_4O_{10}(OH)_2 + 1.32\ H^+ + 4.78\ H_2O = 0.78\ Al_2Si_2O_5(OH)_4 + 0.25\ Mg^{2+} + 0.25\ Fe^{2+} + 0.16\ Ca^{2+} + 2.44\ H_4SiO_4^\circ$

8. $Ca_{.16}(Al_{1.56}Mg_{.25}Fe_{.25})Si_4O_{10}(OH)_2 + 0.41\ K^+ + 0.57\ H^+ + 2.64\ H_2O =$

$$0.68\ K_{.6}Mg_{.25}Al_{2.3}Si_{3.5}O_{10}(OH)_2 + 0.08\ Mg^{2+} + 0.25\ Fe^{2+} + 0.16\ Ca^{2+} + 1.62\ H_4SiO_4^\circ$$

9. $K_{.6}Mg_{.25}Al_{2.3}Si_{3.5}O_{10}(OH)_2 + 1.1\ H^+ + 3.15\ H_2O = 1.15\ Al_2Si_2O_5(OH)_4 + 0.6\ K^+ + 1.2\ H_4SiO_4^\circ + 0.25\ Mg^{2+}$

10. $NaAlSi_5O_{12} \cdot 4\ H_2O + Ca^{2+} + Al(OH)_4^- = CaAl_2Si_4O_{12} \cdot 4\ H_2O + Na^+ + H_4SiO_4^\circ$

11. $CaCO_3 + 2\ Al(OH)_4^- + 4\ H_4SiO_4^\circ + 2\ H^+ = CaAl_2Si_4O_{12} \cdot 4\ H_2O + 8\ H_2O + H_2CO_3^\circ$

Note: All reactions written with Al immobile.

Table 2. Compositions of key minerals

1. Quartz SiO_2
2. Calcite $CaCO_3$
3. Ferroan calcite $Ca_{.95}Fe_{.05}CO_3$
4. Albite $NaAlSi_3O_8$
5. K-feldspar $KAlSi_3O_8$
6. Intermediate plagioclase $Na_{.7}Ca_{.3}Al_{1.3}Si_{2.7}O_8$
7. Kaolinite $Al_2Si_2O_5(OH)_4$
8. Chlorite $Mg_{2.3}Fe_{2.3}Al_{2.8}Si_{2.6}O_{10}(OH)_8$
9. Ca-montmorillonite $Ca_{.16}(Al_{1.56}Mg_{.25}Fe_{.25})Si_4O_{10}(OH)_2$
10. Na-montmorillonite $Na_{.33}(Al_{1.56}Mg_{.25}Fe_{.25})Si_4O_{10}(OH)_2$
11. Illite $K_{.6}Mg_{.25}Al_{2.3}Si_{3.5}O_{10}(OH)_2$
12. Laumontite $CaAl_2Si_4O_{12} \cdot 4H_2O$
13. Clinoptilolite $NaAlSi_5O_{12} \cdot 4H_2O$
14. Sphene $Ca(Ti_{.7}Al_{.4})SiO_5$

Table 3. Hydrolysis reactions

1. $SiO_2 + 2\ H_2O = H_4SiO_4^\circ$
2. $CaCO_3 = Ca^{2+} + CO_3^{2-}$
3. $Ca_{.95}Fe_{.05}CO_3 = 0.95\ Ca^{2+} + 0.05\ Fe^{2+} + CO_3^{2-}$
4. $NaAlSi_3O_8 + 8\ H_2O = Na^+ + Al(OH)_4^- + 3\ H_4SiO_4^\circ$
5. $KAlSi_3O_8 + 8\ H_2O = K^+ + Al(OH)_4^- + 3\ H_4SiO_4^\circ$
6. $Na_{.7}Ca_{.3}Al_{1.3}Si_{2.7}O_8 + 8\ H_2O = 0.7\ Na^+ + 0.3\ Ca^{2+} + 1.3\ Al(OH)_4^- + 2.7\ H_4SiO_4^\circ$
7. $Al_2Si_2O_5(OH)_4 + 7\ H_2O = 2\ Al(OH)_4^- + 2\ H_4SiO_4^\circ + 2\ H^+$
8. $Mg_{2.3}Fe_{2.3}Al_{2.8}Si_{2.6}O_{10}(OH)_8 + 3.6\ H_2O + 6.4\ H^+ = 2.3\ Mg^{2+} + 2.3\ Fe^{2+} + 2.8\ Al(OH)_4^- + 2.6\ H_4SiO_4^\circ$
9. $Ca_{.16}(Al_{1.56}Mg_{.25}Fe_{.25})Si_4O_{10}(OH)_2 + 10.24\ H_2O = 0.16\ Ca^{2+} + 1.56\ Al(OH)_4^- + 0.25\ Fe^{2+} + 0.25\ Mg^{2+} + 4\ H_4SiO_4^\circ + 0.24\ H^+$
10. $Na_{.33}(Al_{1.56}Mg_{.25}Fe_{.25})Si_4O_{10}(OH)_2 + 10.24\ H_2O = 0.33\ Na^+ + 1.56\ Al(OH)_4^- + 0.25\ Mg^{2+} + 0.25\ Fe^{2+} + 4\ H_4SiO_4^\circ + 0.24\ H^+$
11. $K_{.6}Mg_{.25}Al_{2.3}Si_{3.5}O_{10}(OH)_2 + 11.2\ H_2O = 0.6\ K^+ + 2.3\ Al(OH)_4^- + 3.5\ H_4SiO_4^\circ + 0.25\ Mg^{2+} + 1.2\ H^+$
12. $CaAl_2Si_4O_{12} \cdot 4\ H_2O + 8\ H_2O = Ca^{2+} + 2\ Al(OH)_4^- + 4\ H_4SiO_4^\circ$
13. $NaAlSi_5O_{12} \cdot 4\ H_2O + 8\ H_2O = Na^+ + Al(OH)_4^- + 5\ H_4SiO_4^\circ$
14. $Ca(Ti_{.7}Al_{.4})SiO_5 + 2\ H_2O + 2.3\ H^+ = Ca^{2+} + 0.7\ TiOOH^+ + 0.4\ Al(OH)_4^- + H_4SiO_4^\circ$

Table 4. Reaction pairs

1. $CaCO_3 + 0.05\ Fe^{2+} = Ca_{.95}Fe_{.05}CO_3 + 0.05\ Ca^{2+}$

2. $2\ KAlSi_3O_8 + 2\ H^+ + 9\ H_2O = Al_2Si_2O_5(OH)_4 + 2\ K^+ + 4\ H_4SiO_4°$

3. $KAlSi_3O_8 + Na^+ = NaAlSi_3O_8 + K^+$

4. $Na_{.7}Ca_{.3}Al_{1.3}Si_{2.7}O_8 + 0.6\ Na^+ + 1.2\ H_4SiO_4° = 1.3\ NaAlSi_3O_8 + 0.3\ Ca^{2+} + 2.4\ H_2O$

5. $Na_{.7}Ca_{.3}Al_{1.3}Si_{2.7}O_8 + 1.3\ H^+ + 3.45\ H_2O = 0.65\ Al_2Si_2O_5(OH)_4 + 0.3\ Ca^{2+} + 0.7\ Na^+ + 1.4\ H_4SiO_4°$

6. $1.4\ Al_2Si_2O_5(OH)_4 + 2.3\ Mg^{2+} + 2.3\ Fe^{2+} + 6.2\ H_2O = Mg_{2.3}Fe_{2.3}Al_{2.8}Si_{2.6}O_{10}(OH)_8 + 0.2\ H_4SiO_4° + 9.2\ H^+$

7. $Ca_{.16}(Al_{1.56}Mg_{.25}Fe_{.25})Si_4O_{10}(OH)_2 + 1.32\ H^+ + 4.78\ H_2O = 0.78\ Al_2Si_2O_5(OH)_4 + 0.25\ Mg^{2+} + 0.25\ Fe^{2+} + 0.16\ Ca^{2+} + 2.44\ H_4SiO_4°$

8. $Ca_{.16}(Al_{1.56}Mg_{.25}Fe_{.25})Si_4O_{10}(OH)_2 + 0.41\ K^+ + 0.57\ H^+ + 2.64\ H_2O =$

   $0.68\ K_{.6}Mg_{.25}Al_{2.3}Si_{3.5}O_{10}(OH)_2 + 0.08\ Mg^{2+} + 0.25\ Fe^{2+} + 0.16\ Ca^{2+} + 1.62\ H_4SiO_4°$

9. $K_{.6}Mg_{.25}Al_{2.3}Si_{3.5}O_{10}(OH)_2 + 1.1\ H^+ + 3.15\ H_2O = 1.15\ Al_2Si_2O_5(OH)_4 + 0.6\ K^+ + 1.2\ H_4SiO_4° + 0.25\ Mg^{2+}$

10. $NaAlSi_5O_{12} \cdot 4\ H_2O + Ca^{2+} + Al(OH)_4^- = CaAl_2Si_4O_{12} \cdot 4\ H_2O + Na^+ + H_4SiO_4°$

11. $CaCO_3 + 2\ Al(OH)_4^- + 4\ H_4SiO_4° + 2\ H^+ = CaAl_2Si_4O_{12} \cdot 4\ H_2O + 8\ H_2O + H_2CO_3°$

Note: All reactions written with Al immobile.

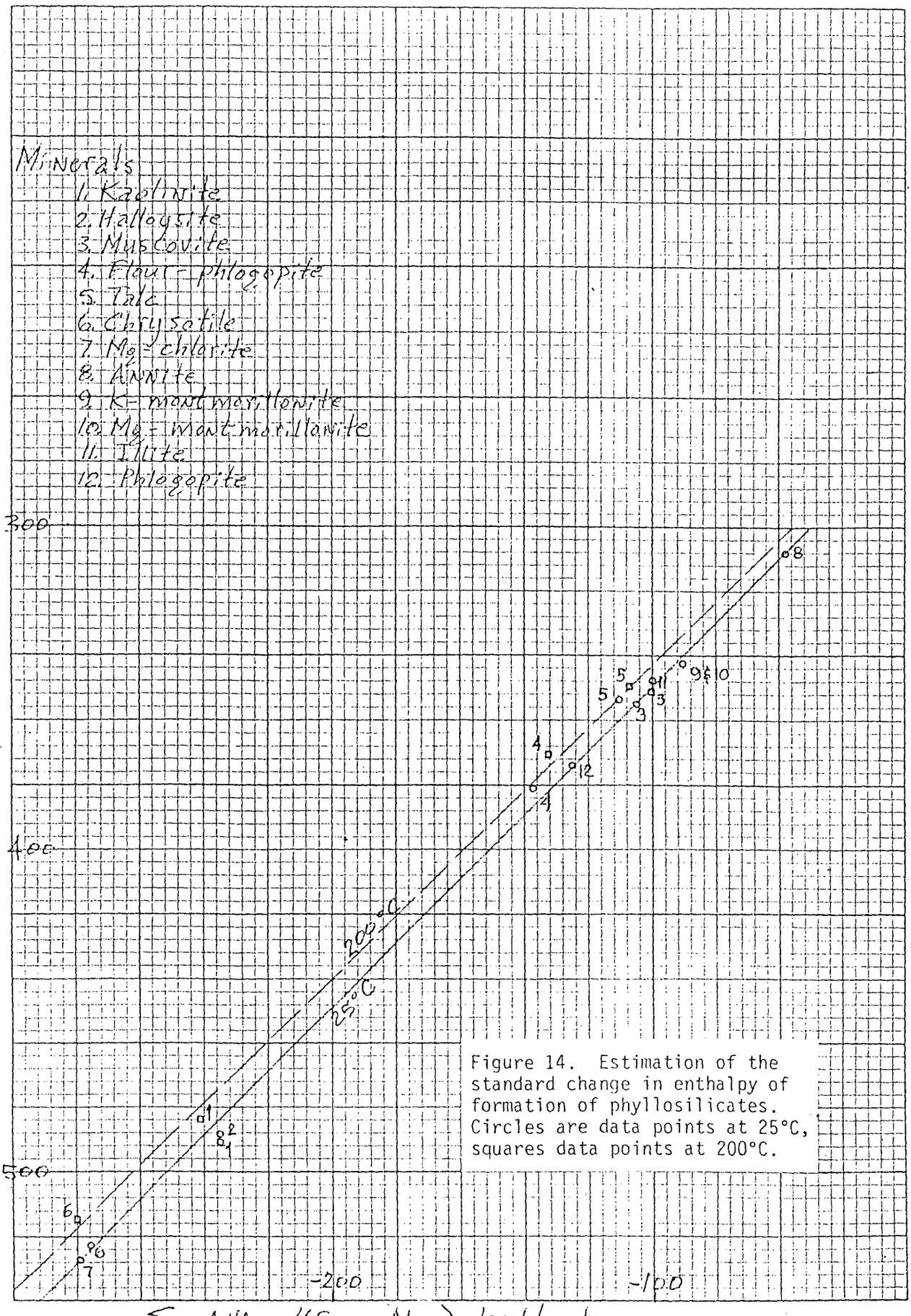

Figure 14. Estimation of the standard change in enthalpy of formation of phyllosilicates. Circles are data points at 25°C, squares data points at 200°C.

46 0782

and divided by ($Si_{Tet}+Al_{Tet}$). A surprisingly good fit for all available phyllosilicate data can be made with a straight line. The standard change in entropy ($\Delta S°_f$) is calculated from the relationship, $S°_{abs} - S°_f = \Delta S°_f$. Absolute entropy ($S°_{abs}$) is estimated by summing the oxide constituents where water is treated as ice. The entropy of formation ($S°_f$) is calculated by summing elemental entropies. Accordingly, $\Delta H°_f$ and $\Delta S°_f$ at 25°C for Ca-montmorillonite are -1352 kcal/mole and -294 cal/degmole, respectively. Thus, $\Delta G°_f$ is -1264.4 kcal/mole at 25°C from the relationship, $\Delta G°_f = \Delta H°_f - T\Delta S°_f$. Using a method suggested by Tardy and Garrels (1974) $\Delta G°_f$ at 25°C is estimated at -1257.2 kcal/mole. Enthalpies can be calculated at higher temperatures using average heat capacity data (Helgeson, 1969) to prepare curves for the appropriate temperature (fig. 14). Values of entropies for oxides and elements at higher temperatures can be interpolated from Robie and others (1978).

Ferroan Calcite

The calculation of $\Delta G°_f$ for ferroan calcite (and intermediate plagioclase) (table 2) is essentially the estimation of $\Delta G°_f$ for solid solutions. Ferroan calcite is considered a mixture in which calcite and siderite are pure end members. For solid solution,

$$\Delta G°_f = X_1 \Delta G°_{f,1} + X_2 \Delta G°_{f,2} + RT\,(X_1 \ln X_1 + X_2 \ln X_2)$$

where X_1, and X_2 are the mole fractions of component 1 and 2, respectively and $\Delta G°_{f,1}$ and $\Delta G°_{f,2}$ are the standard change in free energies of formation for components 1 and 2, in this case calcite and siderite. To illustrate the method, $\log K_r$ is calculated for the reaction, $Ca_{.95}Fe_{.05}CO_3 = .95\ Ca^{2+} .05\ Fe^{2+} + CO_3^{2-}$. Calculation of $\Delta G°_f$ at 25°C according to:

$\Delta G°_f = X_{CaCO_3}\Delta G°_{fCaCO_3} + X_{FeCO_3}\ \Delta G°_{fFeCO_3} + RT(X_{CaCO_3} \ln X_{CaCO_3} + X_{FeCO_3}\ \ln X_{FeCO_3})$,

with substitution of free energy values and mole fractions, yields a $\Delta G°_f$ = -264.4 kcal/mole. This value is almost identical to a value of -264.3 kcal/mole obtained using an alternative method (Boles, 1978). $\Delta G°_r$ is then +11.59 kcal/mole and therefore log K_r is -8.50.

To estimate $\Delta G°_r$ at higher temperatures requires calculation of $\Delta H°_r$. $\Delta S°_f$ = -62.53 cal/degmole, since $S°_{abs}$ of ferroan calcite calculated from the oxides is 22.17 cal/degmole and $S°_f$ from the elements is 84.70 cal/degmole. For ferroan calcite $\Delta H°_f$ = -283.03 kcal/mole, from the relationship $\Delta H°_f = \Delta G°_f + T\Delta S°_f$, and therefore $\Delta H°_r$ is -2.91 kcal/mole. Assuming $\Delta H°_r$ is constant over the temperature range of 25 to 200°C, log K_r can be calculated from the Van't Hoff equation:

$$\log K_T = -\frac{\Delta H°_r}{2.303R}\left(\frac{1}{T} - \frac{1}{298}\right) + \log K_{298}$$

where T is in degrees Kelvin. Under these assumptions log K_r at 100°C is -8.95 for ferroan calcite and -8.73 for calcite.

Thermodynamically, calcite at pH less than about 8 is more soluble than ferroan calcite. Solutions with a Ca^{2+}/Fe^{2+} ratio less than 1.41 will first yield ferroan calcite. Predictably, then in shales, iron-bearing carbonate might be favored, since the smectite/illite transformation (table 4) yields a Ca^{2+}/Fe^{2+} ratio of 0.64. Indeed, energy dispersive analysis shows authigenic carbonate to be iron-bearing (fig. 9).

REFERENCES

Boles, J. R., 1978, Active ankerite cementation in the subsurface Eocene of southwest Texas: Contributions to Mineralogy and Petrology, v. 68, p. 13-22.

Freed, R. L., 1980, Shale mineralogy and burial diagenèsis in four geoopressured wells, Hidalgo and Brazoria Counties, Texas, in Loucks, R. G., Richmann, D. L., and Milliken, K. L., Factors controlling reservoir quality in Tertiary sandstones and their significance to geopressured geothermal production: U.S. Department of Energy, Division of Geothermal Energy Report DOE/ET/27111-1, Appendix A, p. 111-172.

Helgeson, H. C. 1969, thermodynamics of hydrothermal systems at elevated temperatures and pressures: American Journal of Science, v. 267, p. 729-804.

Loucks, R. G., Richmann, D. L., and Milliken, K. L., 1980, Factors controlling reservoir quality in Tertiary sandstones and their significance to geopressured geothermal production: U.S. Department of Energy, Division of Geothermal Energy Report DOE/ET/27111-1, 188 p.

Robie, R. A., Hemingway, B. S., and Fisher, J. R., 1978, Thermodynamic properties of minerals and related substances at 298.15K and 1 bar (10^5 Pascals) pressure and at higher temperatures: U.S. Geological Survey Bulletin 1452, 456 p.

Tardy, Y., and Garrels, R. M., 1974, A method of estimating the Gibbs energies of formation of layer silicates: Geochimica et Cosmochimica Acta, v. 38, p. 1101-1116.

Travena, A. S., and Nash, W. P., An electron microprobe study of detrital feldspar: submitted to Journal of Sedimentary Petrology.